Recycled carbon fibre mats for interlayer toughening of carbon fibre/epoxy composites

Quan, Dong; Farooq, Ujala; Zhao, Guoqun; Dransfeld, Clemens; Alderliesten, René

DOI
10.1016/j.matdes.2022.110671

Publication date
2022

Document Version
Final published version

Published in
Materials and Design

Materials & Design 218 (2022) 110671

Contents lists available at ScienceDirect

Materials & Design

journal homepage: www.elsevier.com/locate/matdes

Recycled carbon fibre mats for interlayer toughening of carbon fibre/epoxy composites

Dong Quan [a,b,*], Ujala Farooq [b], Guoqun Zhao [a], Clemens Dransfeld [b], René Alderliesten [b,*]

[a] Key Laboratory for Liquid-Solid Structural Evolution and Processing of Materials (Ministry of Education), Shandong University, China
[b] Department of Aerospace Structures and Materials, Delft University of Technology, Netherlands

HIGHLIGHTS

- Recycled carbon fibres were used for laminate interlayer toughening.
- The commingled rCFs/Polyphenylene-sulfid fibres showed excellent toughening performance.
- The mode-I and mode-II fracture energies of the laminate significantly increased by 220% and 105%, respectively.
- This study demonstrated interlayer toughening an attractive application for recycled carbon fibres.

GRAPHICAL ABSTRACT

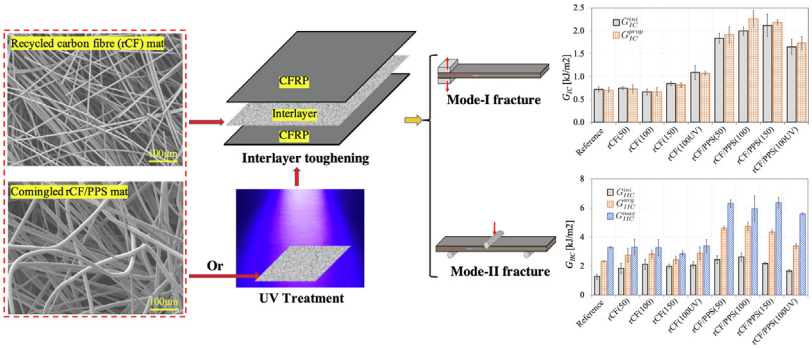

ARTICLE INFO

Article history:
Received 12 November 2021
Revised 13 April 2022
Accepted 14 April 2022
Available online 20 April 2022

Keywords:
Polymer-matrix composites (PMCs)
Recycling
Interlayer toughening
Fracture toughness
Toughening mechanisms

ABSTRACT

Exploring routes for the effective use of recycled carbon fibres (rCFs) is critical to close the loop in the life cycle of carbon fibres. This work demonstrated a potential of using rCFs for interlayer toughening of carbon fibre/epoxy composites. Nonwoven mats based on rCFs and commingled rCFs/Polyphenylene-sulfid (PPS) fibres were used to interlay a laminate, aiming to improve the mode-I and mode-II fracture toughness. The experimental results proved significant enhancements in the interlaminar fracture properties upon interleaving, with the rCF/PPS mats exhibiting a more prominent toughening effectiveness than the rCF mats. For example, the maximum increase in mode-I and mode-II fracture initiation energies of the laminates was 51% and 66%, respectively upon interleaving the rCF mats, and 220% and 105%, respectively by adding the rCFs/PPS mats. The fractography analysis proved that the main toughening mechanisms were fibre debonding and pulling-out for the rCF mats and fibre bridging for the commingled rCFs/PPS mats. The differences in the toughening mechanisms resulted in opposite effects of the interlayer/epoxy adhesion to the fracture toughness, i.e. an improved interlayer/epoxy adhesion increased the toughening effectiveness of the rCF mats, but negatively affected the toughening performance of the rCF/PPS mats.

1. Introduction

Carbon fibre composites possessed excellent combination of properties, such as high stiffness and strength, good fatigue and corrosion resistance, high design flexibility and light weight. For these reasons, the applications of carbon fibre composites have

* Corresponding authors at: Key Laboratory for Liquid-Solid Structural Evolution and Processing of Materials (Ministry of Education), Shandong University, China (D. Quan).
E-mail addresses: quandong@sdu.edu.cn (D. Quan), R.C.Alderliesten@tudelft.nl (R. Alderliesten).

https://doi.org/10.1016/j.matdes.2022.110671
0264-1275/

extensively expanded in a wide range of industries over the last two decades, including the aerospace, automotive, wind energy and sport sectors. Consequently, the amount of composite waste has simultaneously increased to a significant level that poses concerns about environmental pollution. Recycling is the most efficient way of managing composite waste, particularly if we consider that carbon fibres preserve high intrinsic value [1,2]. In recent years, a number of techniques have been developed to reclaim carbon fibres from CFRP waste, including pyrolysis, solvolysis, and a fluidized bed process [3,4]. Typically, recycled carbon fibres (rCFs) can maintain nearly all the mechanical properties of the virgin fibers [3,5,6], but in a short and random form. While some of the techniques for fibre reclamation are entering into a mature stage [5], it is equally critical to explore routes for effective use of recycled carbon fibres (rCFs).

Interlayer toughening is one of the most prevalent and effective methods for interlaminar toughening of carbon fibre composites. To date, a wide range of materials have been employed for interlayer toughening of laminates, including thermoplastic fibres [7–9], thermoplastic films [10,11], thermoplastic powder [12], stainless steel fibres [13], carbon nanotubes (CNTs) [14,15], graphene [16,17] and short carbon/glass fibres [18,19]. While these interlayer materials exhibited different advantage and disadvantages, different levels of toughness improvements were obtained. Considering the high flexibility in interlayer selection, interlayer toughening of laminates is an attractive and high-value outlet of rCFs, that offers a potential of using rCFs in semi-critical or critical loading-bearing structures. Even though the usage of rCFs for interlayer toughening has not been investigated yet, many researchers have already used virgin short carbon fibres for interlayer toughening [20–23]. Xu et al. [20] reported that G_{IC} and G_{IIC} of a laminate were increased by 99% and 109%, respectively due to interleaving short carbon fibres. The main toughening mechanisms were observed to be the pull-out and debonding of the short carbon fibres from the surrounding epoxy matrix. Additionally, the out-of-plane and in-plane electrical conductivity of the laminate was increased by 82% and 96%, respectively. Lee et al. [21,22] systematically studied the effects of interleaving short carbon fibres on the mechanical and fracture properties of a laminate. It was reported that the addition of short carbon fibre interlayers slightly increased G_{IC} by 28% [22], and significantly increased G_{IIC} by 260% [21]. Based on these studies, it is clear that interleaving short carbon fibres has a potential to noticeably increase the interlaminar fracture toughness of the laminates. However, the toughening performance and mechanisms of rCFs can be very different as virgin short carbon fibres, as they possess different surface sizing, fibre orientation and fibre length distribution. For this reason, it is desirable to investigate the toughening performance and mechanisms of rCFs while they are used as toughening interlayers of laminates. Additionally, among different interlayer materials, thermoplastic fibres have proved an outstanding toughening performance, i.e. it was reported that the addition of nonwoven thermoplastic fibres increased the mode-I fracture energy (G_{IC}) and mode-II fracture energy (G_{IIC}) of carbon fibre composites by more than 200% [24–27]. Accordingly, it is also attractive to investigate the toughening performance of interlayers consisting of both rCFs and thermoplastic fibres, that can potentially further improve the toughening performance of rCFs.

In the light of the above considerations, this work aimed to investigate the potential of using rCF products for interlayer toughening of carbon fibre/epoxy composites, with the effects of interlayer/epoxy adhesion being also studied. Nonwoven mats based on discontinuous rCFs and commingled rCFs/PPS fibres were used as interlayer materials of a laminate. The effects of the adhesion between the interlayers and the epoxy matrix of the laminates were investigated. The mode-I and mode-II fracture behaviour of the interleaved laminates were studied using a double cantilever beam (DCB) test and an end-notched flexure (ENF) test, respectively. The toughening mechanisms of the rCF mats and the rCF/PPS mats were also carefully investigated.

2. Experimental

2.1. Materials

The epoxy resin was EPIKOTE Resin 04908 with an epoxy equivalent weight of 165 g/equiv., and the curing agent was EPIKURE Curing Agent 04908 with an amine equivalent weight of 50 g/equiv.. They were supplied by HEXION, Netherlands. The carbon fibres were twill-weave fabrics with an areal density of 650 g/m^2 from TenCate, Netherlands. The recycled carbon fibre (rCF) mats and commingled rCF/PPS fibre mats were supplied by ELG Carbon Fibre Ltd, UK. The rCFs were recovered from aerospace-grade laminate waste from Airbus using a pyrolysis process, during which, the sizing on the rCFs had been removed. The weight content of the PPS fibres in the rCF/PPS mats was 60%. The average length of the recycled carbon fibres and the PPS fibres was 80 mm with a range between 60–100 mm. An areal density of 50 g/m^2, 100 g/m^2 and 150 g/m^2 was chosen for both of the rCF mats and the rCF/PPS mats. Fig. 1 shows typical microscopy images of the commingled rCF/PPS mats, and the average diameter of the rCFs and the PPS fibres was measured to be 5.8$\pm$ 0.3μm and 15.7$\pm$0.5 μm, respectively.

2.2. Processing and characterisation of the laminates

In this work, both of original and UV-treated rCF and rCF/PPS mats were used as interlayers. The UV-treatment was carried out to increase the surface activity of the interlayers, and hence enhance their adhesion with the epoxy matrix. The rCF and rCF/PPS mats were treated using three 30 W tube UVC-lamps, that were installed 50 mm apart within an enclosed chamber (with a volume of 550 mm$\times$170 mm$\times$60 mm). After the top side of the mat (facing the UV lamps) was treated for 10 mins, the mat was then inverted to treat its opposite side for another 10 mins. It should be noted that the UV-treatment process was determined based on a series of trials to ensure no significant property degradation of the PPS fibres upon the treatment. Raman spectroscopy point analysis was conducted on the rCFs and a PPS film (the same grade of PPS polymer as the PPS fibres) before and after the UV-treatment using an inVia Confocal Raman microscope from Renishaw, UK.

The laminates were manufactured using a vacuum-assisted resin infusion process, as schematically shown in Figs. 2(a-d). A layup consisting of eight plies of carbon fibre fabrics and an interlayer between the 4th and 5th plies was prepared. A layer of PTFE film with a thickness of 12.7 μm was also inserted at the mid-plane to generate crack starters within the fracture testing specimens. The layup was then sealed in a vacuum bag and infused with the epoxy matrix at room temperature. The laminates were cured for 12 h at room temperature under vacuum before they were placed in a pre-heated oven at 80 °C for another 6 h. The average thickness of the reference laminate was measured to to be 4.96 mm, and the average thickness of the interleaved laminates varied with the areal density of the interlayers, as shown in Section 3.1. The fibre volume fraction of the reference laminate was 50.4$\pm$0.8%, that was calculated based on three measurements using the Rule of Mixtures for the density. The cured laminate were then machined into specimens for a mode-I double cantilever beam (DCB) test [28] and a mode-II end-notched flexure (ENF) test [29] test. The dimensions and testing setups of the DCB and ENF tests are shown in Figs. 2(e) and (f). The testes were carried out using a Zwick/Roell ZO10 testing machine at a constant displacement rate of 3 mm/min and 0.5 mm/min for the DCB test and the ENF test,

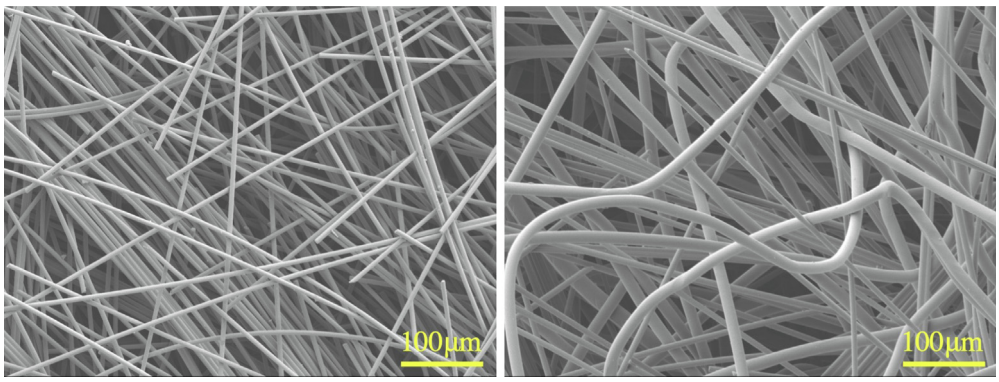

Fig. 1. Typical microscopy images of the rCF mats and commingled rCF/PPS mats.

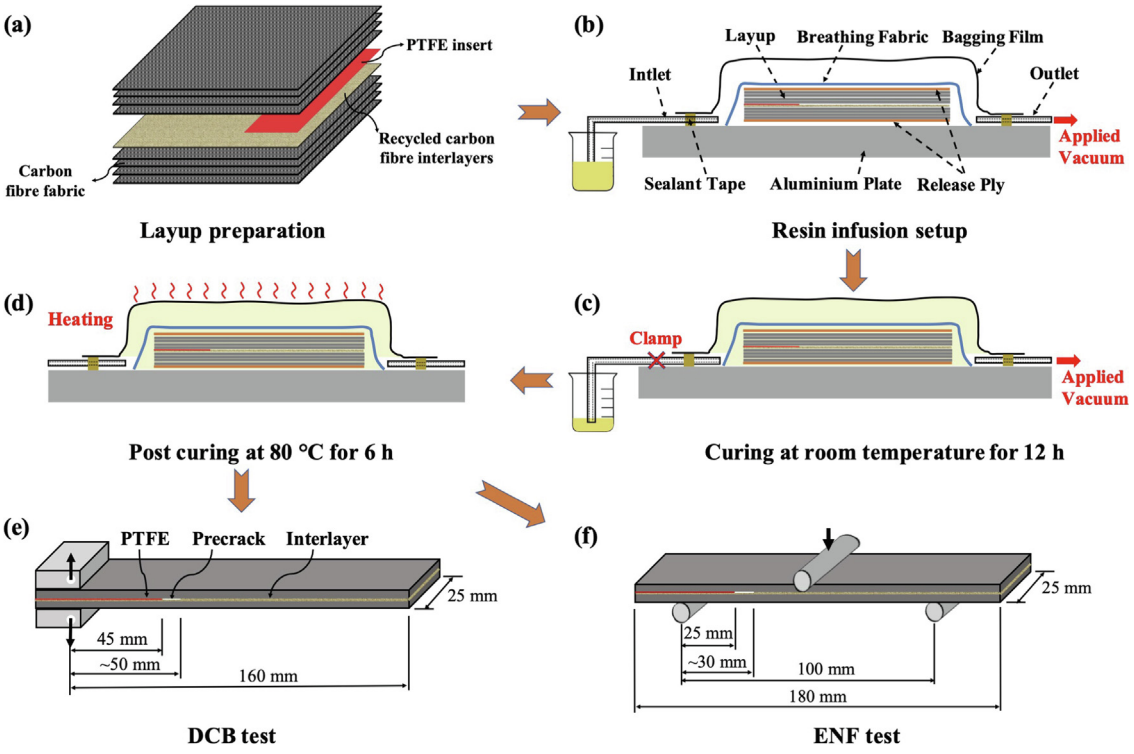

Fig. 2. Schematics for illustrating the laminate manufacturing process and mode-I and mode-II fracture toughness measurements.

respectively. A high resolution digital camera was used to measure the length of the crack during the tests. To create a sharp crack at the crack tip, a precrack with a length of about 5 mm from the front of the crack starter was introduced by applying an opening load to the DCB and ENF specimens. Three replicate tests were conducted for each set. The side-views of the DCB and ENF specimens before and after the tests were imaged using a VK-X1000 microscope from KEYENCE Corporation, and the fracture surfaces were analysed using a scanning electron microscope (SEM, JOEL JSM-7500F).

3. Results and discussion

3.1. Characterisation of the interlayers

Fig. 3 shows the Raman spectrum curves of the rCFs and PPS before and after the UV-treatment, with the the corresponding peaks labeled. It was observed that applying a UV-treatment to the rCFs formed a number of polar functional groups, including ether group (C—O), carbonyl group (C=O) and aldehyde group (O=C—H) next to the characteristic D and G band gaps attributed to the graphitic structure of the fibres. The formation of functional groups upon applying UV-treatment to carbon fibres had also been observed in the literature [30], and the treatment efficiency was reported to be affected by the UV output, the fibre composition and structure and the air flow during the UV-treatment. Similarly, additional C—O and C=O groups were also generated in the molecular structure of the PPS polymer upon the UV-treatment. During the surface treatment process, the UV light provided sufficient energy to break the C—C/C—H species, which resulted in subsequent oxidation reactions [31]. The presence of polar functional groups on the surfaces of the rCFs and PPS fibres significantly improved their adhesion with the epoxy matrix of the laminate, that was confirmed by the SEM analysis on the fracture surfaces of the laminates in Sections 3.2 and 3.3.

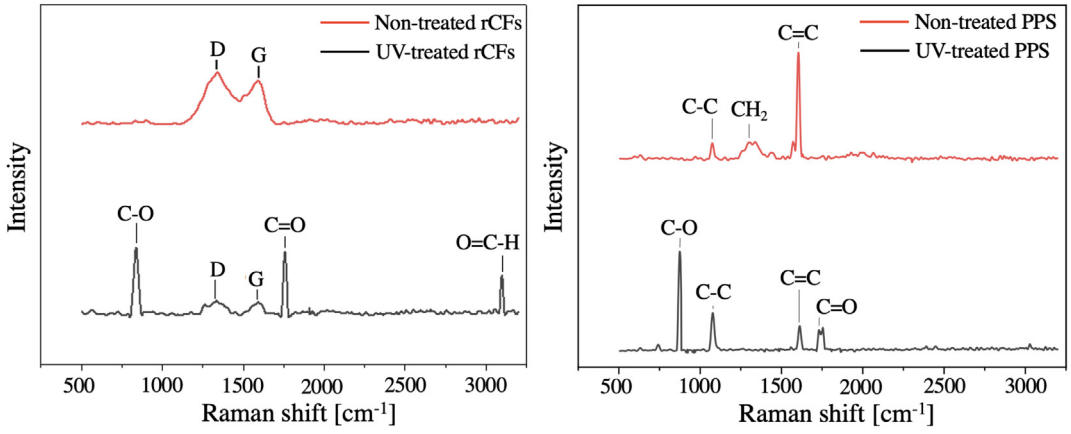

Fig. 3. Raman spectrum curves of the rCFs and PPS before and after the UV-treatment.

Fig. 4 shows microscopy images of the cross-sections of the interleaved laminates. The yellow double-head arrows indicate the interlayers. In Fig. 4 and the rest of this paper, the interlayers were referred to as the type of the materials followed by the areal density in the bracket, e.g. rCF(100) represents the rCF mat with an areal density of 100 g/m^2 and rCF(100UV) means the rCF(100) mat was UV-treated. No visible air-bubble in the interlayers was observed in all the cases, indicating a thorough impregnation of the interlayers by the epoxy matrix. The average thicknesses of the interlayers based on 20 measurements using an ImageJ software are summarised in Table 1. One can see that the rCF/PPS interlayers possessed a higher thickness than their rCF counterparts with the same areal densities. This was due to the lower density of the PPS fibres.

3.2. Mode-I fracture behaviour of the laminates

The load versus displacement curves from the DCB tests of the laminates are shown in Fig. 5. A stick–slip fracture behaviour of the DCB specimens was observed all the laminates studied, that was evidenced by the Zigzag shape of the load–displacement curves. Moreover, no significant changes in the fracture propagation loads of the DCB specimens were observed due to interleaving rCF mats, while the fracture propagation loads had been significantly increased by inserting rCF/PPS mats into the laminates. Fig. 6 shows *R*-curves from the DCB tests of the laminates. It was observed that the mode-I fracture toughness significantly varied with the crack length for all the interleaved laminates. This was due to the local non-uniformity of the length, distribution and orientation of the rCFs in the interlayer mats. The addition of non-treated rCF mats into the laminates had no obvious effects on the values of the *R*-curves, see Fig. 6(a). However, applying a UV-treatment to the rCF(100) mat resulted in noticeable increases of the values on the *R*-curves. Fig. 6(b) shows that the rCF/PPS mats exhibited prominent toughening performance for the laminate. Additionally, in contrast to the rCF(100) mat, the toughening performance of the rCF/PPS(100) mat was negatively affected upon the UV-treatment.

The mode-I fracture initiation energy (G_{IC}^{ini}) and fracture propagation energy (G_{IC}^{prop}) of the laminates are summarised in Fig. 7. One can see that interleaving rCF(50) and rCF(100) mats into the laminate failed to improve the mode-I fracture energies, and a slight improvement of 17% in G_{IC}^{ini} and 16% in G_{IC}^{prop} was obtained by increasing the areal density of the rCF mats to 150 g/m^2.

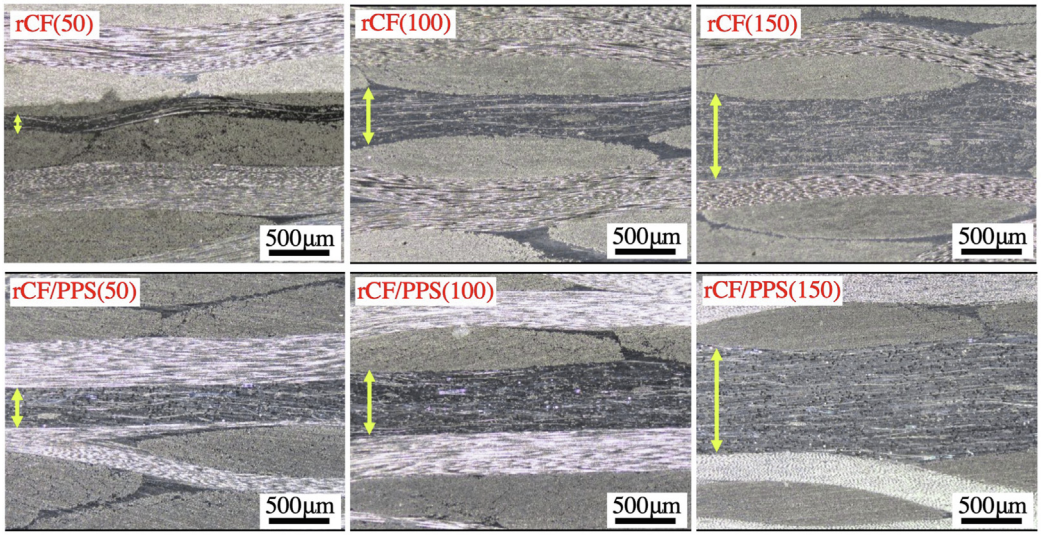

Fig. 4. Side-view of the interleaved laminates. The yellow double-head arrows indicate the interlayers.

Table 1
Average thicknesses of the interlayers within the cured laminates.

Laminates	rCF(50) μm	rCF(100) μm	rCF(150) μm	rCF/PPS(50) μm	rCF/PPS(100) μm	rCF/PPS(150) μm
Thickness	166±18	334±59	621±80	287±26	524±47	811±79

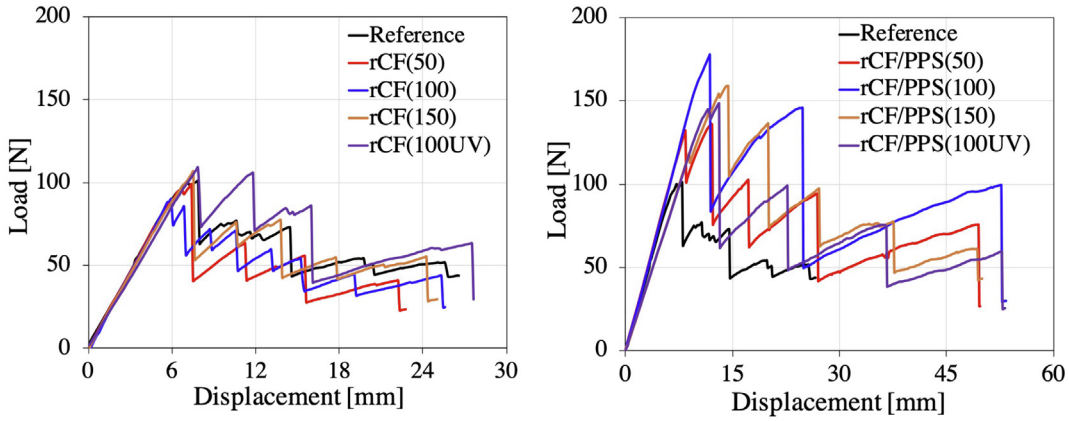

Fig. 5. The load versus displacement curves from the DCB tests of the laminates.

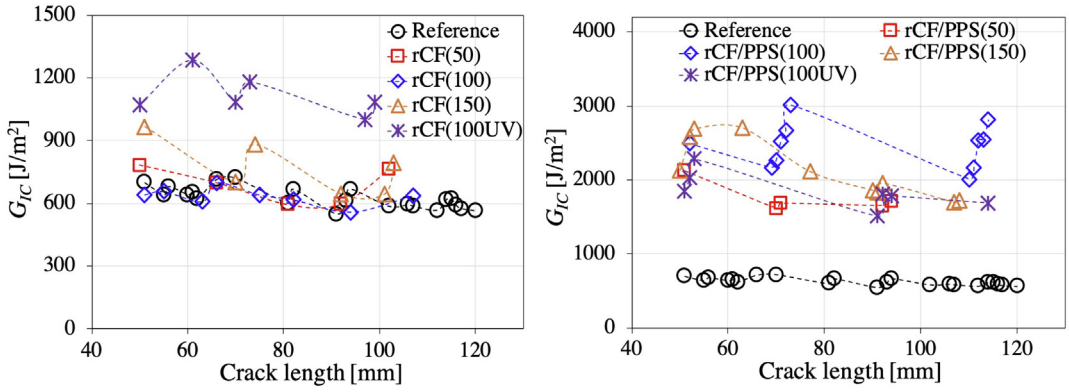

Fig. 6. Representative *R*-curves from the DCB tests on the laminates.

Applying a UV-treatment to the rCF(100) mat noticeably improved its toughening performance, i.e. G_{IC}^{ini} and G_{IC}^{prop} increased by 51% and 52%, respectively by interleaving the rCF(100UV) mat. The incorporation of the rCF/PPS interlayers resulted in prominent increases in G_{IC} of the laminates. In particular, G_{IC}^{ini} significantly increased from 719 J/m^2 of the reference laminate to 1841 J/m^2 (by 156%) upon interleaving the rCF/PPS(50) mat, and then steadily increased to 2119 J/m^2 (by 195%) as the areal density of the rCF/PPS mat increased to 150 g/m^2. Similarly, G_{IC}^{prop} increased from 707 J/m^2 of the reference laminate to a maximum value of 2260 J/m^2 (by 220%) by interleaving the rCF/PPS(100) mat and then remained more or less the same as the areal density of the rCF/PPS mat increased to 150 g/m^2. However, the application of the UV-treatment to the rCF/PPS(100) mat decreased G_{IC}^{ini} and G_{IC}^{prop} by 17% and 24%, respectively. In general, the toughening performance of the non-treated rCFs for the mode-I fracture mode was poor when compared to original short carbon fibres that were used in the literature [20,22,32]. This was due to the relatively poor adhesion between the rCFs and the epoxy matrix, since the recycling process removed the sizing on the carbon fibre surfaces. An increased surface activity of the rCFs upon the UV-treatment enhanced the adhesion at the rCF/epoxy interface (as shown in Fig. 3), that improved the toughening effectiveness of the UV-treated rCFs to a level that was higher than the original short carbon fibres in the literature [22,32]. Encouragingly, the commingled rCFs/PPS fibres exhibited a much higher toughing performance than the original short carbon fibres [20,22,32] and the ones decorated with carbon nanotube and graphene [33–35]. This obviously represents a potential application of the commingled rCFs/PPS fibres for laminate toughening.

Fig. 8 presents representative photographs of the fracture surfaces and side-view images of the crack paths for the DCB specimens. The red colour dashed lines indicate the fronts of the PTFE inserts. Numerous rCFs were observed on both sides of the fracture surfaces for the laminate interleaved with non-treated and

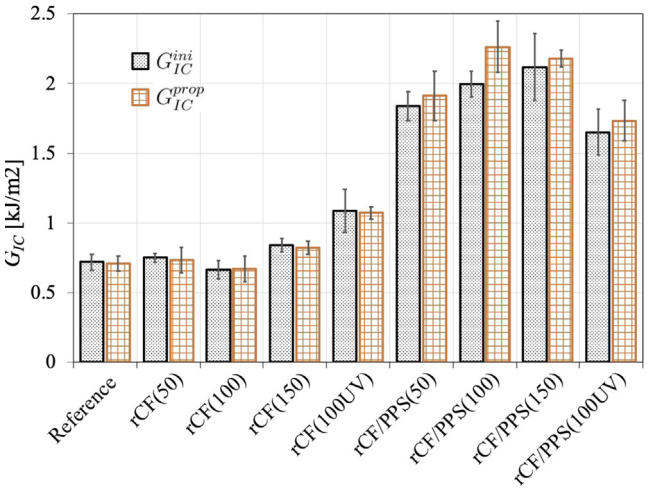

Fig. 7. A summary of the mode-I fracture initiation energy (G_{IC}^{ini}) and fracture propagation energy (G_{IC}^{prop}) of the laminates.

UV-treated rCF(100) mat, as shown in Fig. 8(a). This indicated that the fracture took place essentially in the middle of the interlayers in both cases, as shown in the corresponding side-view images. Fig. 8(b) shows that the crack also propagated more or less in the middle of the interlayers for the laminates interleaved with non-treated rCF/PPS mats, that left both sides of the fracture surfaces covered with the interlayer materials. However, applying the UV-treatment to the rCF/PPS mat transformed the failure mode to a mixture of cohesive failure inside the interlayer (in the middle of the DCB specimens) and interfacial failure at the interlayer/laminate interface (at the two edges of the DCB specimens). It should be noted that the physical fracture processes are driven by the intense local stresses around crack tip, and hence the crack typically propagates along the path that possessed the weakest strength during the mode-I fracture process. In this case, the enhanced interlayer/epoxy adhesion improved the failure strength of the rCF/PPS interlayers and subsequently resulted in the transition of the failure modes.

Representative SEM images of the fracture surfaces for the DCB specimens are shown in Fig. 9. The image for the reference laminate focused on the carbon fibre bundles oriented vertically to the crack propagation direction. It was clear that extensive carbon fibre debonding and breakage took place during the fracture process of the reference laminate (see Fig. 9(a)), yielding a relatively high G_{IC}^{prop} (707 J/m^2). The fracture surfaces of the laminates interleaved with rCF(100) and rCF(100UV) mats appeared more or less the same, i.e. both of them were featured with a large number of debonded and pulled-out rCFs (as shown in Fig. 9(b) and (c)). Hence, the main toughening mechanisms of the rCF mats were rCF debonding and pulling-out. The application of the UV-treatment to the rCF mats enhanced the adhesion between the rCFs and the epoxy matrix (see Section 3.1), and subsequently increased the required force for the debonding and pulling-out of rCFs from the epoxy matrix. This improved the toughness contribution of the rCF debonding and pulling-out mechanisms, and increased the mode-I fracture energies of the laminates (as observed in Fig. 7). A large number of debonded and pulled-out PPS fibres and rCFs were also observed on the fracture surfaces of the laminates interleaved with rCF/PPS mats (see Fig. 9(d)). Nevertheless, unlike the carbon fibres on the fracture surfaces of the rCF interleaved laminates, these fibres were in a long and continuous form, that typically indicates the presence of significant fibre bridging during the fracture process. Fibre bridging has proved an effective toughening mechanism for crack resistance [36,24], and hence resulted in excellent toughening performance of the rCF/PPS mats, as shown in Fig. 7. However, applying a UV-treatment to the rCF/PPS mats inhibited the bridging mechanisms of the rCFs and PPS fibres during the fracture process, referring to the much shorter debonded rCFs and PPS fibres in Fig. 9(e)) than those in Fig. 9(d). Moreover, the UV-treatment had also changed the failure mode of the DCB specimens from a pure cohesive failure within the interlayers to partially interfacial failure at the interlayer/laminate interface, as observed in Fig. 8(b). This also led to a decrease in the level of fibre bridging mechanism during the manufacturing process. These phenomenon caused negative effects to the toughening performance of the rCF/PPS mats upon the UV-treatment. Noteworthily, an improved interlayer/epoxy adhesion also led to noticeable damage to the PPS fibres (see Fig. 9(f)), that was not observed for the non-treated PPS fibres. This contributed to the fracture toughness of the laminates interleaved with rCF/PPS mats and avoided a more prominent decrease in the fracture toughness.

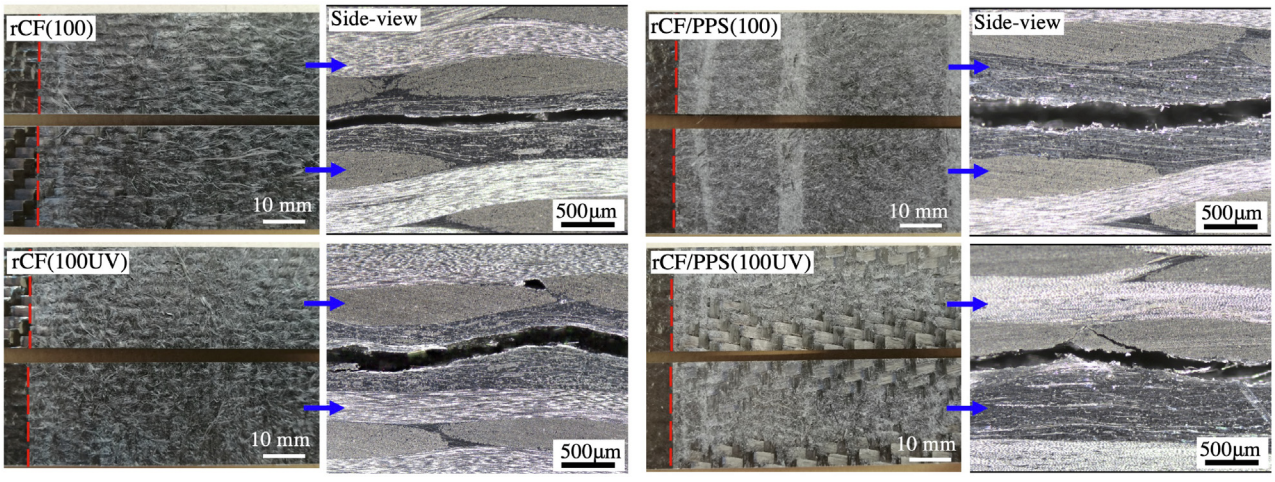

(a) rCF mats (b) rCF/PPS mats

Fig. 8. Representative photographs of the top and bottom fracture surfaces of the DCB specimens and the corresponding side-view images of the crack paths. The red colour dashed lines indicate the fronts of the PTFE inserts.

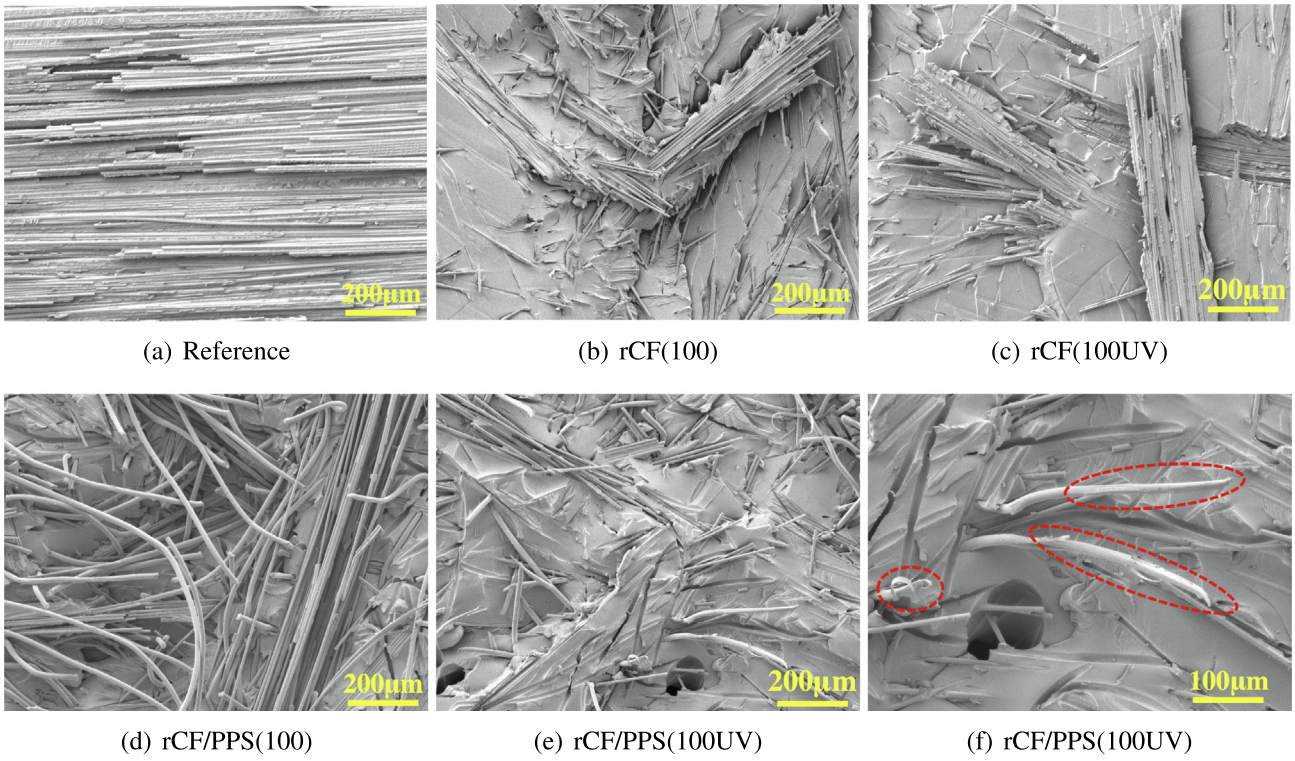

Fig. 9. Representative SEM images of the mode-I fracture surfaces. The red colour dashed ovals in (f) indicate the damaged PPS fibres.

3.3. Mode-II fracture behaviour of the laminates

Fig. 10 shows representative load versus displacement curves from the ENF tests of the laminates. It can be seen that the maximum crack propagation load increased due to interleaving in all the cases, with the rCF/PPS interlayers exhibiting a more prominent effect. Representative mode-II *R*-curves of the laminates from the ENF tests are shown in Fig. 11. A 'rising' *R*-curve behaviour, i.e. the fracture energy increased steadily with the crack length, was observed for all the studied laminates. This indicates an extension in the length of the fracture damage zone at the crack tip vicinity [37], i.e. the region featured with fibre bridging mechanisms behind the crack tip became longer as the crack propagating forward. For the reference laminate, the crack propagated slowly to a crack length of 45 mm, at where the ENF test was terminated. The addition of the rCF interlayers resulted in an unstable crack propagation behaviour, i.e. the crack grew slowly at the beginning of the test and then suddenly speeded up and failed the ENF specimen. This explained why there were less data points on the *R*-curves of the laminates interleaved with rCF mats in Fig. 11(a). It was obvious that the mode-II fracture toughness of the rCF interleaved laminates was higher than the reference laminate at the initiation stage of the fracture. Moreover, an improved rCF/epoxy adhesion upon the UV-treatment had negligible effect on the *R*-curve of the laminates interleaved with rCF(100) mat. Encouragingly, Fig. 11(b) shows that interlaying rCF/PPS mats into the laminates resulted in a much sharper rising trend of the *R*-curves. This phenomenon typically indicates the presence of extensive fibre bridging mechanism during the fracture process, as will be confirmed later on. However, applying a UV-treatment to the rCF

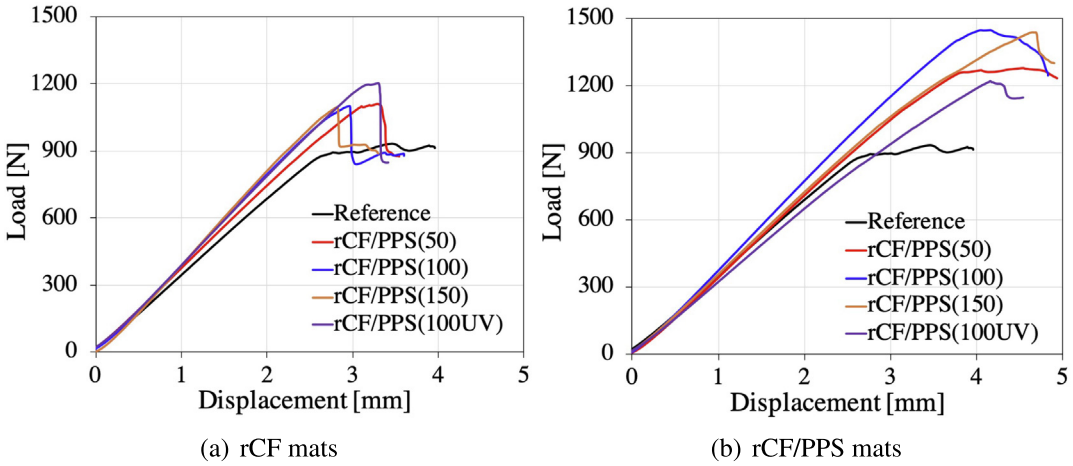

Fig. 10. The load versus displacement curves from the ENF tests of the laminates.

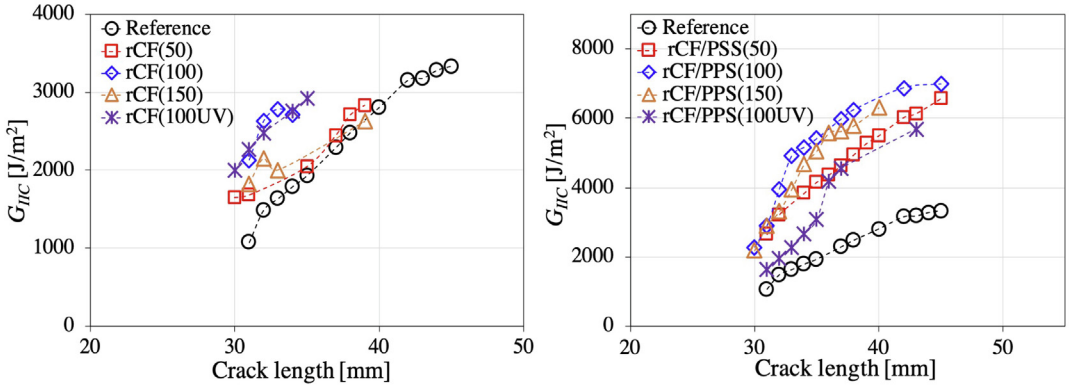

(a) rCF mats (b) rCF/PPS mats

Fig. 11. Representative *R*-curves from the ENF tests on the laminates.

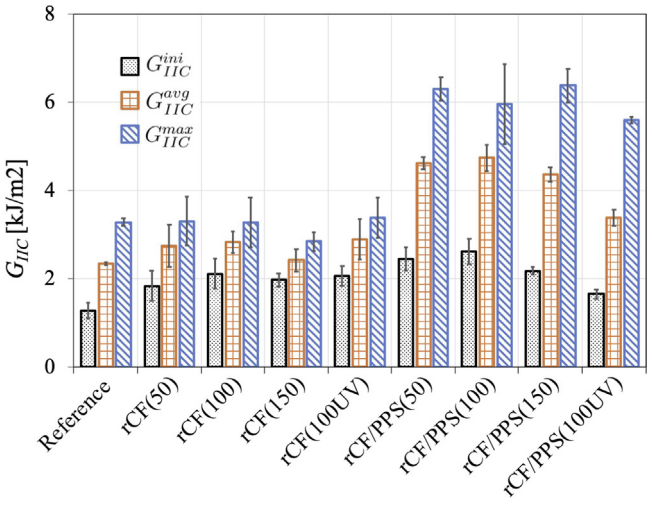

Fig. 12. A summary of the mode-II fracture initiation energy (G_{IIC}^{ini}) and average values (G_{IIC}^{avg}) and maximum values (G_{IIC}^{max}) of the mode-II *R*-curves of the laminates.

(100) mat caused an obvious drop in the *R*-curve values of the corresponding laminate.

The mode-II fracture initiation energy (G_{IIC}^{ini}), average values (G_{IIC}^{avg}) and maximum values (G_{IIC}^{max}) of the *R*-curves are shown in Fig. 12. Overall, the areal densities of the rCF and rCF/PPS mats had no significant effect on the mode-II fracture toughness of the laminates. The addition of the rCF mats into the laminate noticeably increased G_{IIC}^{ini} by 44%, 66% and 55% for the rCF(50), rCF(100) and rCF(150) mats, respectively. However, no obvious increases in G_{IIC}^{avg} and G_{IIC}^{max} were observed by interleaving these rCF mats. This was caused by the unstable crack propagation of the rCF interleaved laminates, i.e. the specimens failed dynamically after the crack propagated a few millimetres. Additionally, the application of a UV-treatment to the rCF(100) mat had no effect on the mode-II fracture energies of the interleaved laminate. More prominent increases in the mode-II fracture energies were observed by interleaving the rCF/PPS mats into the laminates. For instance, interleaving the rCF/PPS(100) mat into the reference laminate increased G_{IIC}^{ini}, G_{IIC}^{avg} and G_{IIC}^{max} by 105%, 103% and 82%, respectively.

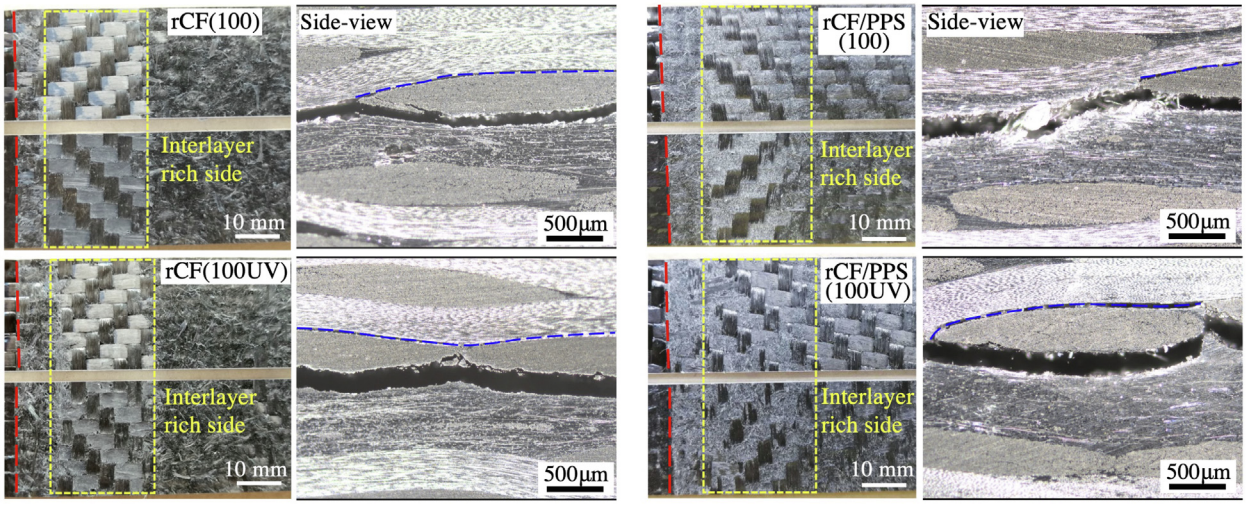

(a) rCF mats (b) rCF/PPS mats

Fig. 13. Representative photographs of the top and bottom fracture surfaces of the ENF specimens and the corresponding side-view images of the crack paths. The red colour dashed lines denote the fronts of the PTFE inserts, the yellow colour dashed boxes indicate the region of mode-II fracture propagation, and the blue colour dashed lines denote debonded carbon fibre bundles.

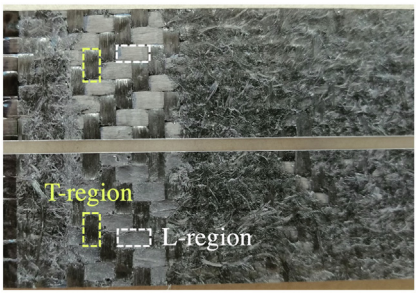

Fig. 14. A pair of fracture surfaces of a tested ENF specimen for defining the L-regions (yellow dashed box) and T-regions (white dashed box).

Applying a UV-treatment to the rCF/PPS(100) mat detrimentally affected the mode-II fracture energies of the rCF/PPS(100) interleaved laminate, i.e. the percentage increases of G_{IIC}^{ini}, G_{IIC}^{avg} and G_{IIC}^{max} considerably dropped to 29%, 45% and 71%, respectively upon the UV-treatment. The percentage increases of G_{IIC} due to interlaying non-treated rCF/PPS mats were comparable to a value of 109% due to interleaving original short carbon fibres in [20], but much lower than a value of 260% in [22]. Nevertheless, it is worthy to mention that G_{IIC}^{max} of the laminates interleaved with original carbon fibres in [22] were approximately 4000 J/m^2, which were much lower than G_{IIC}^{max} of the laminates interleaved with non-treated and UV-treated rCF/PPS mats in this study.

Representative photos of the fracture surfaces and corresponding side-view images of the ENF specimens are shown in Fig. 13. The red colour dashed lines denote the fronts of the PTFE inserts, the yellow colour dashed boxes indicate the region of mode-II fracture propagation, and the blue colour dashed lines denote debonded carbon fibre bundles that orientated vertically to the crack propagation direction. For clarification, the region between the red dashed line and the yellow dashed box was the pre-crack and the area after the yellow dashed box was the section that was separated by hand after the testing. It was observed that the mode-II failure occurred at the interlayer/laminate interface vicinity for all the interleaved laminates, leaving the entire or the majority of the interlayers on one side of the fracture surfaces, i.e. the interlayer rich sides of the fracture surfaces in Fig. 13. This explained why the areal densities of the rCF and rCF/PPS interlayers had no obvious effect on the mode-II fracture energies of the laminates, as shown in Fig. 12. For an easy discussion, the fracture surfaces of the laminates were divided into L-regions and T-regions in Fig. 14, referring to the regions with a carbon fibre direction that was longitudinal and transverse to the crack propagation direction, respectively. By taking a closer look at the photos in Fig. 13, it was observed that the T-regions on both sides of the fracture surfaces were covered with dark colour carbon fibres for all the interleaved laminates. This corresponded to the delamination of the transverse carbon fibre bundles on the side-view images, as indicated by the red dashed lines in Fig. 13. The main difference in the fracture topography between different interleaved laminates were within the L-regions. For the laminates interleaved with non-treated and UV-treated rCF mats, the entire interlayer attached to the interlayer rich side of the fracture surfaces, while only bare carbon fibres were observed on the opposite side, see Fig. 13(a). For the laminates interleaved with non-treated and UV-treated rCF/PPS mats, the majority of the interlayer was left on the interlayer rich side of the fracture surfaces in the L-regions, leaving a small amount of PPS fibres and rCFs on the opposite side, as shown in Fig. 13(b).

Fig. 15 shows representative SEM images of the mode-II fracture surfaces of the laminates. Extensive carbon fibre debonding and breakage were observed within the T-regions of the reference laminate (Fig. 15(a)), and the addition of interlayers had no effect to the fracture mechanisms within the T-regions in all the cases

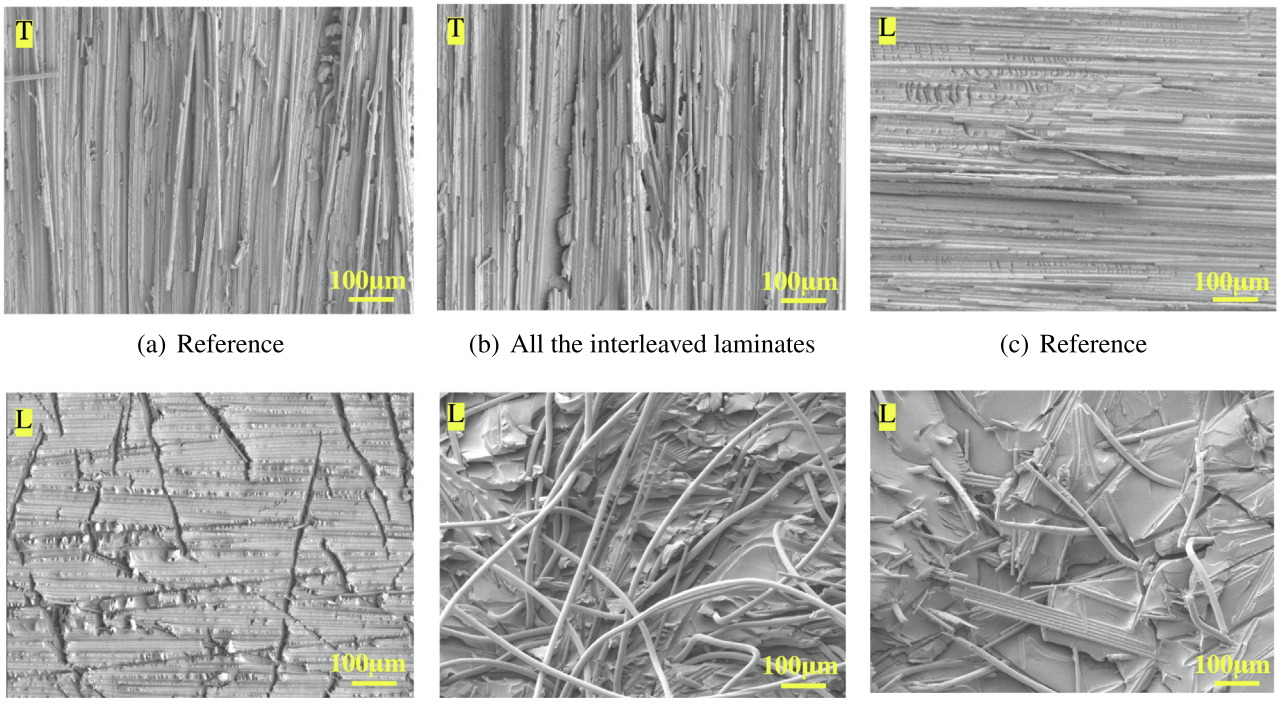

Fig. 15. Representative SEM images of the fracture surfaces of the ENF specimens. (a) and (b) focus on the T-regions of the fracture surfaces. (c)-(f) focus on the L-regions of the interlayer-rich sides of the fracture surfaces. L and T positions are referred to Fig. 14.

(Fig. 15(b)). This confirmed that the varied mode-II fracture properties of different laminates were mainly attributed to the different fracture mechanisms within the L-regions. For the reference laminate, evidence of significant carbon fibre debonding and breakage was also observed within the L-regions, see Fig. 15(c). For the laminates interleaved with original and UV-treated rCF mats, the L-regions of the interlayer-rich sides of the fracture surfaces were covered with a layer of peeled-off epoxy matrix with many crack lines and carbon fibre imprints (see Fig. 15(d)). This indicates that the crack propagated at the epoxy/carbon fibre interface during the mode-II fracture process, that was associated with carbon fibre debonding from the epoxy matrix and generation of micro-cracks within the epoxy layers. This type of failure mode inhibited carbon fibre debonding and breakage mechanisms and resulted in the relatively poor toughening performance of the non-treated and UV-treated rCF mats, as shown in Fig. 12. Evidence of significant bridging mechanisms of rCFs and PPS fibres was observed on the fracture surfaces of the laminate interleaved with non-treated rCF/PPS mats, i.e. numerous debonded rCFs and PPS fibres in a long form presented on the fracture surfaces of rCF/PPS interleaved laminate, see Fig. 15(e). These mechanisms contributed to the excellent toughening performance of the rCF/PPS mats. However, an improved adhesion at the interlayer/epoxy interface upon the UV-treatment caused considerable drops in the level of debonding and bridging mechanisms of the rCFs and PPS fibres, evidenced by the relatively well-embedded rCFs and PPS fibres in Fig. 15(f). This caused the negative effect to the mode-II fracture energies of the laminates that was shown in Fig. 12.

4. Conclusions

This work aims to explore the potential of using recycled carbon fibres (rCFs) as interlayers to enhance the interlaminar fracture toughness of carbon fibre/epoxy composites. Herein, nonwoven mats based on rCFs and commingled rCFs/PPS fibres were used for the interlayer toughening of a laminate, aiming to improve the mode-I and mode-II fracture toughness.

In general, the toughening performance of the original rCF mats was relatively poor. The addition of rCF mats only resulted in a maximum increase of 17% and 16% in the mode-I fracture initiation energy (G_{IC}^{ini}) and mode-I fracture propagation energy (G_{IC}^{prop}) of the laminate, respectively. For the mode-II fracture, adding rCF interlayers noticeably increased the fracture initiation energy (G_{IIC}^{ini}) by 66% for maximum, but failed to improve the average values (G_{IIC}^{avg}) and maximum values (G_{IIC}^{max}) of the *R*-curves. Fortunately, the application of the UV-treatment to the rCF mats obviously improved its overall toughening performance, e.g. G_{IC}^{ini} and G_{IIC}^{ini} were increased by 51% and 62%, respectively upon interleaving the UV-treated rCF mats with an areal density of 100 g/m^2. The addition of original and UV-treated rCF mats inhibited the significant carbon fibre delamination and bridging mechanisms, which occurred during the mode-I and mode-II fracture behaviour of the reference laminate. This caused detrimental effects to the toughness enhancement, and led to the relatively low levels of toughening effectiveness of the rCF mats. Encouragingly, the commingled rCFs with PPS fibres resulted in significant improvement of the toughening performance. Interleaving rCF/PPS mats led to a maximum increase of 195% and 220% for the G_{IC}^{ini} and G_{IC}^{prop} of the laminate, respectively. It also significantly increased G_{IIC}^{ini}, G_{IIC}^{avg} and G_{IIC}^{max} of the laminate by 105%, 103% and 95%, respectively. However, applying a UV-treatment to the rCF/PPS mats negatively affected the toughening performance of the commingled mats.

Noteworthily, an improved interlayer/epoxy adhesion exhibited obvious effects on the toughening effectiveness of the interlayers, that was significantly different for the rCF mats and the rCF/PPS mats. The different effects of interlayer/epoxy adhesion were mainly attributed to the different toughening mechanisms of the interlayers. In this study, the main toughening mechanisms of the rCF mats were determined to be the debonding and pulling-out of rCFs from the epoxy for the mode-I fracture of the composites. In this case, the improved interlayer/epoxy adhesion increased the required force for the fibre debonding and pulling-out from the epoxy, and hence significantly enhanced the mode-I toughening performance of the rCF mats. The toughness improvements upon interleaving the rCF/PPS mats were mainly attributed to the extensive debonding and subsequent bridging of the rCFs and PPS fibres during the mode-I and mode-II fracture process. However, the improved interlayer/epoxy adhesion hampered these mechanisms and caused detrimental effects to the toughening performance of the commingled mats. These observations have clearly proved that the interlayer/epoxy adhesion is a critical factor, that should be carefully considered for the development of strong and tough composites using the interlay toughening technique.

Overall, this work revealed that the incorporation of UV-treated rCF mats and commingled rCF/PPS mats are promising to enhance the interlaminar fracture properties of carbon fibre/epoxy composites. A potential of using these recycled carbon fibre products for critical and semi-critical structures by hybridising them with continuous carbon fibre composites has been demonstrated.

Data Availability

The raw/processed data required to reproduce these findings cannot be shared at this time as the data also forms part of an ongoing study.

Declaration of Competing Interest

The authors declare that they have no known competing financial interests or personal relationships that could have appeared to influence the work reported in this paper.

Acknowledgements

The authors would like to acknowledge the financial supports from the key research and development program of Shandong Province (Grant No. 2021ZLGX01). Dong Quan is grateful to the funding from the European Union's Horizon 2020 research and innovation programme under the Marie Skłodowska-Curie grant agreement No. 842467.

References

[1] S. Job, Recycling composites commercially, Reinf. Plast. 58 (5) (2014) 32–38, https://doi.org/10.1016/S0034-3617(14)70213-9.
[2] G. Cai, M. Wada, I. Ohsawa, S. Kitaoka, J. Takahashi, Interfacial adhesion of recycled carbon fibers to polypropylene resin: Effect of superheated steam on the surface chemical state of carbon fiber, Compos. Part A: Appl. Sci. Manuf. 120 (2019) 33–40, https://doi.org/10.1016/j.compositesa.2019.02.020.
[3] S. Pimenta, S.T. Pinho, Recycling carbon fibre reinforced polymers for structural applications: Technology review and market outlook, Waste Management 31 (2) (2011) 378–392, environmental Implications of Alternative Materials in Construction and Treatment of Waste. https://doi.org/10.1016/j.wasman.2010.09.019.
[4] J. Zhang, V.S. Chevali, H. Wang, C.-H. Wang, Current status of carbon fibre and carbon fibre composites recycling, Compos. Part B: Eng. 193 (2020) 108053, https://doi.org/10.1016/j.compositesb.2020.108053.
[5] S. Utekar, S. V K, N. More, A. Rao, Comprehensive study of recycling of thermosetting polymer composites-Driving force, challenges and methods, Compos. Part B: Eng. 207 (2021) 108596, https://doi.org/10.1016/j.compositesb.2020.108596.
[6] N. van de Werken, M.S. Reese, M.R. Taha, M. Tehrani, Investigating the effects of fiber surface treatment and alignment on mechanical properties of recycled carbon fiber composites, Compos. Part A: Appl. Sci. Manuf. 119 (2019) 38–47, https://doi.org/10.1016/j.compositesa.2019.01.012.

[7] D. Quan, B. Deegan, R. Alderliesten, C. Dransfeld, N. Murphy, A. Ivankovic, R. Benedictus, The influence of interlayer/epoxy adhesion on the mode-I and mode-II fracture response of carbon fibre/epoxy composites interleaved with thermoplastic veils, Mater. Des. 192 (2020) 108781, https://doi.org/10.1016/j.matdes.2020.108781.
[8] E. Maccaferri, L. Mazzocchetti, T. Benelli, T.M. Brugo, A. Zucchelli, L. Giorgini, Rubbery nanofibrous interleaves enhance fracture toughness and damping of cfrp laminates, Mater. Des. 195 (2020) 109049, https://doi.org/10.1016/j.matdes.2020.109049.
[9] L. Daelemans, A. Cohades, T. Meireman, J. Beckx, S. Spronk, M. Kersemans, I.D. Baere, H. Rahier, V. Michaud, W.V. Paepegem, K.D. Clerck, Electrospun nanofibrous interleaves for improved low velocity impact resistance of glass fibre reinforced composite laminates, Mater. Des. 141 (2018) 170–184, https://doi.org/10.1016/j.matdes.2017.12.045.
[10] J. Yao, T. Zhang, Y. Niu, Effect of curing time on phase morphology and fracture toughness of PEK-C film interleaved carbon fibre/epoxy composite laminates, Compos. Struct. 248 (2020) 112550, https://doi.org/10.1016/j.compstruct.2020.112550.
[11] N. Nash, T. Young, P. McGrail, W. Stanley, Inclusion of a thermoplastic phase to improve impact and post-impact performances of carbon fibre reinforced thermosetting composites - a review, Mater. Des. 85 (2015) 582–597, https://doi.org/10.1016/j.matdes.2015.07.001.
[12] T. Katafiasz, E. Greenhalgh, G. Allegri, S. Pinho, P. Robinson, The influence of temperature and moisture on the mode I fracture toughness and associated fracture morphology of a highly toughened aerospace CFRP, Compos. Part A: Appl. Sci. Manuf. 142 (2021) 106241, https://doi.org/10.1016/j.compositesa.2020.106241.
[13] D. Quan, J.L. Urdaniz, C. Rouge, A. Ivankovic, The enhancement of adhesively-bonded aerospace-grade composite joints using steel fibres, Compos. Struct. 198 (2018) 11–18, https://doi.org/10.1016/j.compstruct.2018.04.071.
[14] Y. Wu, X. Cheng, S. Chen, B. Qu, R. Wang, D. Zhuo, L. Wu, In situ formation of a carbon nanotube buckypaper for improving the interlaminar properties of carbon fiber composites, Mater. Des. 202 (2021) 109535, https://doi.org/10.1016/j.matdes.2021.109535.
[15] T. Meireman, L. Daelemans, E. Van Verre, W. Van Paepegem, K. De Clerck, Nanofibre toughening of dissimilar interfaces in composites, Mater. Des. 195 (2020) 109050, https://doi.org/10.1016/j.matdes.2020.109050.
[16] C.S. Nagi, S.L. Ogin, I. Mohagheghian, C. Crean, A.D. Foreman, Spray deposition of graphene nano-platelets for modifying interleaves in carbon fibre reinforced polymer laminates, Mater. Des. 193 (2020) 108831, https://doi.org/10.1016/j.matdes.2020.108831.
[17] J. Nasser, L. Zhang, H. Sodano, Laser induced graphene interlaminar reinforcement for tough carbon fiber/epoxy composites, Compos. Sci. Technol. 201 (2021) 108493, https://doi.org/10.1016/j.compscitech.2020.108493.
[18] K. Saravanakumar, N. Farouk, V. Arumugam, Effect of fiber orientation on Mode-I delamination resistance of glass/epoxy laminates incorporated with milled glass fiber fillers, Eng. Fract. Mech. 199 (2018) 61–70, https://doi.org/10.1016/j.engfracmech.2018.05.027.
[19] P.K. Gangineni, S. Yandrapu, S.K. Ghosh, A. Anand, R.K. Prusty, B.C. Ray, Mechanical behavior of graphene decorated carbon fiber reinforced polymer composites: An assessment of the influence of functional groups, Compos. Part A: Appl. Sci. Manuf. 122 (2019) 36–44, https://doi.org/10.1016/j.compositesa.2019.04.017.
[20] F. Xu, B. Yang, L. Feng, D. Huang, M. Xia, Improved interlaminar fracture toughness and electrical conductivity of cfrps with non-woven carbon tissue interleaves composed of fibers with different lengths, Polymers 12 (2020) 803, https://doi.org/10.3390/polym12040803.
[21] S.-H. Lee, H. Noguchi, Y.-B. Kim, S.-K. Cheong, Effect of interleaved non-woven carbon tissue on interlaminar fracture toughness of laminated composites: Part I-Mode II, J. Compos. Mater. 36 (18) (2002) 2153–2168, https://doi.org/10.1177/0021998302036018981.
[22] S.-H. Lee, H. Noguchi, Y.-B. Kim, S.-K. Cheong, Effect of interleaved non-woven carbon tissue on interlaminar fracture toughness of laminated composites: Part I-Mode II, J. Compos. Mater. 36 (18) (2002) 2169–2181, https://doi.org/10.1106/002199802026980.
[23] C. Capela, S. Oliveira, J. Ferreira, Fatigue behavior of short carbon fiber reinforced epoxy composites, Compos. Part B: Eng. 164 (2019) 191–197, https://doi.org/10.1016/j.compositesb.2018.11.035.
[24] D. Quan, F. Bologna, G. Scarselli, A. Ivankovic, N. Murphy, Mode-II fracture behaviour of aerospace-grade carbon fibre/epoxy composites interleaved with thermoplastic veils, Compos. Sci. Technol. 191 (2020) 108065, https://doi.org/10.1016/j.compscitech.2020.108065.
[25] D. Quan, F. Bologna, G. Scarselli, A. Ivankovic, N. Murphy, Interlaminar fracture toughness of aerospace-grade carbon fibre reinforced plastics interleaved with thermoplastic veils, Compos. Part A: Appl. Sci. Manuf. 128 (2020) 105642, https://doi.org/10.1016/j.compositesa.2019.105642.
[26] B. Beylergil, M. Tanoglu, E. Aktas, Effect of polyamide-6,6 (PA 66) nonwoven veils on the mechanical performance of carbon fiber/epoxy composites, Compos. Struct. 194 (2018) 21–35, https://doi.org/10.1016/j.compstruct.2018.03.097.
[27] L. Daelemans, S. van der Heijden, I.D. Baere, H. Rahier, W.V. Paepegem, K.D. Clerck, Nanofibre bridging as a toughening mechanism in carbon/epoxy composite laminates interleaved with electrospun polyamide nanofibrous veils, Compos. Sci. Technol. 117 (2015) 244–256, https://doi.org/10.1016/j.compscitech.2015.06.021.
[28] ASTM Standard D5528-13(2013), Standard Test Method for Mode I Interlaminar Fracture Toughness of Unidirectional Fiber-Reinforced Polymer Matrix Composites, ASTM International (2013).
[29] ASTM Standard D7905/D7905M-19(2019), Standard Test Method for Mode II Interlaminar Fracture Toughness of Unidirectional Fiber-Reinforced Polymer Matrix Composites, ASTM International (2019).
[30] S. Osbeck, R. Bradley, C. Liu, H. Idriss, S. Ward, Effect of an ultraviolet/ozone treatment on the surface texture and functional groups on polyacrylonitrile carbon fibres, Carbon 49 (13) (2011) 4322–4330, https://doi.org/10.1016/j.carbon.2011.06.005.
[31] I. Mathieson, R. Bradley, Improved adhesion to polymers by UV/ozone surface oxidation, Int. J. Adhes. Adhes. 16 (1) (1996) 29–31, https://doi.org/10.1016/0143-7496(96)88482-X.
[32] A.R. Ravindran, R.B. Ladani, S. Wu, A.J. Kinloch, C.H. Wang, A.P. Mouritz, The electric field alignment of short carbon fibres to enhance the toughness of epoxy composites, Compos. Part A: Appl. Sci. Manuf. 106 (2018) 11–23, https://doi.org/10.1016/j.compositesa.2017.12.006.
[33] A.R. Ravindran, R.B. Ladani, S. Wu, A.J. Kinloch, C.H. Wang, A.P. Mouritz, Multi-scale toughening of epoxy composites via electric field alignment of carbon nanofibres and short carbon fibres, Compos. Sci. Technol. 167 (2018) 115–125, https://doi.org/10.1016/j.compscitech.2018.07.034.
[34] J. Cheon, M. Kim, Impact resistance and interlaminar shear strength enhancement of carbon fiber reinforced thermoplastic composites by introducing MWCNT-anchored carbon fiber, Compos. Part B: Eng. 217 (2021) 108872, https://doi.org/10.1016/j.compositesb.2021.108872.
[35] H. Nie, Z. Xu, B. Tang, C. Dang, Y. Yang, X. Zeng, B. Lin, X. Shen, The effect of graphene oxide modified short carbon fiber on the interlaminar shear strength of carbon fiber fabric/epoxy composites, J. Mater. Sci. 56 (2021) 488–496, https://doi.org/10.1007/s10853-020-05286-y.
[36] D. Quan, C. Mischo, X. Li, G. Scarselli, A. Ivankovic, N. Murphy, Improving the electrical conductivity and fracture toughness of carbon fibre/epoxy composites by interleaving MWCNT-doped thermoplastic veils, Compos. Sci. Technol. 182 (2019) 107775, https://doi.org/10.1016/j.compscitech.2019.107775.
[37] B. Blackman, A. Kinloch, M. Paraschi, The determination of the mode II adhesive fracture resistance, G_{IIC}, of structural adhesive joints: an effective crack length approach, Eng. Fract. Mech. 72 (6) (2005) 877–897, https://doi.org/10.1016/j.engfracmech.2004.08.007.